

*Citation for published version:*

Almond, DP & Pickering, SG 2012, 'An analytical study of the pulsed thermography defect detection limit', *Journal of Applied Physics*, vol. 111, no. 9, 093510. <https://doi.org/10.1063/1.4704684>

*DOI:*

[10.1063/1.4704684](https://doi.org/10.1063/1.4704684)

*Publication date:*

2012

*Document Version*

Publisher's PDF, also known as Version of record

[Link to publication](https://doi.org/10.1063/1.4704684)

Copyright (2012) American Institute of Physics. This article may be downloaded for personal use only. Any other use requires prior permission of the author and the American Institute of Physics. The following article appeared in Almond, D. P. and Pickering, S. G., 2012. An analytical study of the pulsed thermography defect detection limit. *Journal of Applied Physics*, 111 (9), 093510, and may be found at <http://dx.doi.org/10.1063/1.4704684>

**University of Bath**

## **Alternative formats**

If you require this document in an alternative format, please contact:  
[openaccess@bath.ac.uk](mailto:openaccess@bath.ac.uk)

### **General rights**

Copyright and moral rights for the publications made accessible in the public portal are retained by the authors and/or other copyright owners and it is a condition of accessing publications that users recognise and abide by the legal requirements associated with these rights.

### **Take down policy**

If you believe that this document breaches copyright please contact us providing details, and we will remove access to the work immediately and investigate your claim.

## An analytical study of the pulsed thermography defect detection limit

D. P. Almond and S. G. Pickering

Citation: *J. Appl. Phys.* **111**, 093510 (2012); doi: 10.1063/1.4704684

View online: <http://dx.doi.org/10.1063/1.4704684>

View Table of Contents: <http://jap.aip.org/resource/1/JAPIAU/v111/i9>

Published by the [American Institute of Physics](#).

---

### Related Articles

Profile of the liquid film wetting a channel  
*Appl. Phys. Lett.* **100**, 074107 (2012)

A remote scanning Raman spectrometer for in situ measurements of works of art  
*Rev. Sci. Instrum.* **82**, 063109 (2011)

Coded excitation for infrared non-destructive testing of carbon fiber reinforced plastics  
*Rev. Sci. Instrum.* **82**, 054902 (2011)

Scatterometry for in situ measurement of pattern reflow in nanoimprinted polymers  
*Appl. Phys. Lett.* **93**, 233105 (2008)

Optimization of the excitation and measurement procedures in nondestructive testing using shearography  
*Rev. Sci. Instrum.* **79**, 115105 (2008)

---

### Additional information on J. Appl. Phys.

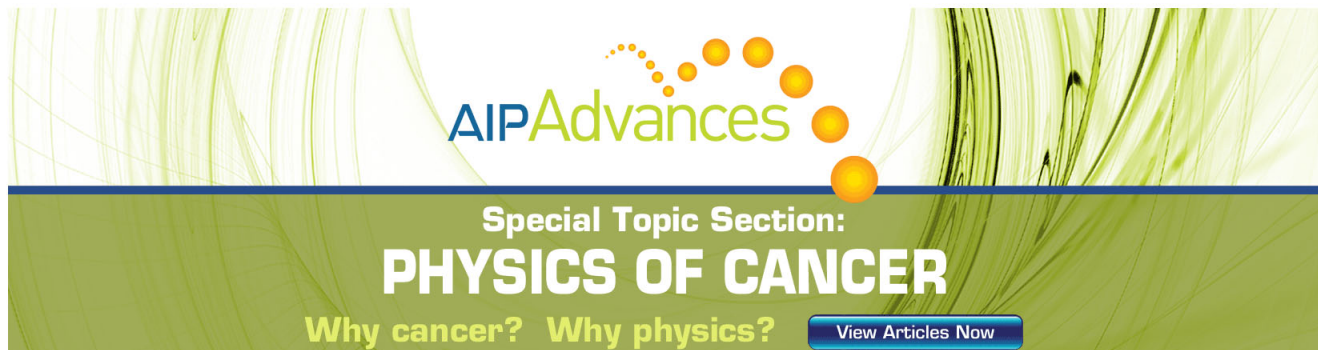
Journal Homepage: <http://jap.aip.org/>

Journal Information: [http://jap.aip.org/about/about\\_the\\_journal](http://jap.aip.org/about/about_the_journal)

Top downloads: [http://jap.aip.org/features/most\\_downloaded](http://jap.aip.org/features/most_downloaded)

Information for Authors: <http://jap.aip.org/authors>

## ADVERTISEMENT

The advertisement features a green background with abstract, flowing, wavy lines in a lighter green shade. At the top, the text 'AIPAdvances' is displayed in a green, sans-serif font. Below this, the text 'Special Topic Section:' is written in a smaller, white, sans-serif font. The main title 'PHYSICS OF CANCER' is prominently displayed in a large, bold, white, sans-serif font. Below the title, the text 'Why cancer? Why physics?' is written in a smaller, white, sans-serif font. In the bottom right corner, there is a blue button with the text 'View Articles Now' in white.

# An analytical study of the pulsed thermography defect detection limit

D. P. Almond and S. G. Pickering

UK Research Centre in NDE (RCNDE), Department of Mechanical Engineering, University of Bath, Claverton Down, Bath BA2 7AY, United Kingdom

(Received 6 December 2011; accepted 14 March 2012; published online 3 May 2012)

A simple modification of the one-dimensional expression for the thermal contrast of a layer provides a useful prediction of peak contrast temperature and contrast peak time for defects of all aspect ratios. The new analytical results have been shown to agree with numerical modelling. The thermographic nondestructive evaluation (NDE) rule-of-thumb that defects are detected if aspect ratio exceeds two is shown to have no general validity as peak contrast is found to depend critically on defect depth and absorbed excitation energy as well as defect aspect ratio. The effects of thermal diffusivity anisotropy are included in the analysis and illustrated by simulations of defect image contrast in composite materials. © 2012 American Institute of Physics. [<http://dx.doi.org/10.1063/1.4704684>]

## I. INTRODUCTION

Pulse transient thermography or flash thermography was the earliest developed<sup>1–3</sup> and is now the most widely used form of thermographic nondestructive testing/evaluation. It involves flash heating the surface of the part under inspection using a high energy optical flash lamp, or lamps, and monitoring the subsequent surface cooling with an infrared camera. Defects lying in a plane parallel to and below the surface block the conduction of heat into the part, causing a reduction in the cooling rate at surface above the defect that may be revealed by an IR camera. Proven applications of the technique include the detection of: adhesion failures of surface coatings, particularly, thermal barrier coatings; delamination defects in composite materials, including impact damage and bond-line defects between adhesively bonded parts. The technique has the attractions: of being rapid; non-contacting; of providing a simple clear image of a defective area; of being applicable to a very wide range of materials; and of being largely unaffected by the geometry of the part under inspection. However, the technique is generally considered to be only suitable for “near surface” defects and there has been a long established “rule-of-thumb” that the “defect aspect ratio” (defect diameter/defect depth) should exceed two. Whilst there is general agreement amongst practitioners that the above rule-of-thumb characterises the limitations on defect detection sensitivity, there has been remarkably little research into its physical origins. The purpose of this paper is to present a simple analytical formulation that characterises the technique’s defect detection capabilities and that exposes the shortcomings of the rule-of-thumb.

## II. THEORY

The impulse heating response of a semi-infinite half space is given by the well known expression<sup>4</sup>

$$T(x, t) = \frac{J_0}{\sqrt{\pi \rho c k t}} e^{-\frac{x^2}{4\alpha t}} \quad (1)$$

in which  $T(x, t)$  is the temperature rise at a depth  $x$  beneath the surface at a time  $t$  after a uniform impulse of energy  $J_0$  on the surface,  $x = 0$ , at time  $t = 0$ .  $\rho$ ,  $c$ ,  $k$ , and  $\alpha$  are density, heat capacity, thermal conductivity, and thermal diffusivity, respectively.

The response at the surface,  $T(0, t)$ , which may be monitored by an IR camera is obtained by setting  $x = 0$  in Eq. (1).

$$T(0, t) = \frac{J_0}{\sqrt{\pi \rho c k t}} \quad (2)$$

In a flash thermography test,  $J_0$  is the optical energy intensity ( $\text{J/m}^2$ ) from the flash lamp absorbed at the surface that is converted into heat. Equation (2) shows that the magnitude of the heating produced at the surface varies inversely with the effusivity ( $\sqrt{\rho c k}$ ) of the material being impulse heated and that this heat decays with time as  $t^{-0.5}$ . Both the magnitude and the time dependence of the surface temperature,  $T(0, t)$ , are altered by a defects lying beneath the surface in a plane parallel to the surface. Such defects usually take the form of air filled cracks or delaminations that block the conduction of heat from the surface, causing a slower cooling than indicated by Eq. (2). As a first approximation, a region containing a delamination-like defect can be treated as a layer of thickness  $d$ , the depth of the defect below the surface. The impulse heating response of such a layer may be obtained from the expression

$$T(0, t) = \frac{J_0}{\sqrt{\pi \rho c k t}} \left[ 1 + 2 \sum_{n=1}^{\infty} R^n e^{-\frac{(nd)^2}{\alpha t}} \right] \quad (3)$$

Equation (3) was obtained<sup>5,6</sup> from the inverse Laplace function of the convolution of the thermal response function of a layer of thickness  $d$  with a Dirac delta function impulse of magnitude  $J_0$ . The thermal response function of the layer is given by the Bennett and Patty<sup>7</sup> thermal wave interference expression.  $R$  is the effective thermal reflection coefficient of the solid-air interface, which to a very good approximation = 1.

Some insight is obtained by re-expressing Eq. (3) as

$$T(0, t) = \frac{J_0}{\sqrt{\pi\rho ckt}} \left[ \left( 2 + R e^{-\frac{(2d)^2}{4\alpha t}} + R^2 e^{-\frac{(4d)^2}{4\alpha t}} + R^3 e^{-\frac{(6d)^2}{4\alpha t}} + \dots \right) \right] \left( \right) \quad (4)$$

Each of the terms in the inner bracket has the mathematical form of a pulse reflection from an interface a depth  $d$  below the surface having a thermal reflection coefficient  $R$ . The successive terms correspond to the first, second, third, ..., reflections having round-trip paths of lengths  $2d, 4d, 6d, \dots$ , respectively.

The four equations presented above are analytical expressions obtained assuming uniform heating across the surface and subsequent uniform, one-dimensional, thermal conduction into the heated solid. Real defects are finite in their lateral dimensions and heat flow in their vicinity cannot be assumed to be one-dimensional. Previous work by one of the authors<sup>8,9</sup> focused on heat flow around the tip of an in-plane defect and the effect that this had on the apparent size of a defect that might be deduced from flash thermography images. Figure 1(a) illustrates the thermal flux around the tip of a sub-surface in-plane defect. Figure 1(b) shows representative examples<sup>8,9</sup> of the ways that the temperature profiles above and below a finite defect differ from defect-free material at the same depth at a time after the flash heating of the surface. These temperature changes were shown<sup>8,9</sup> to be a

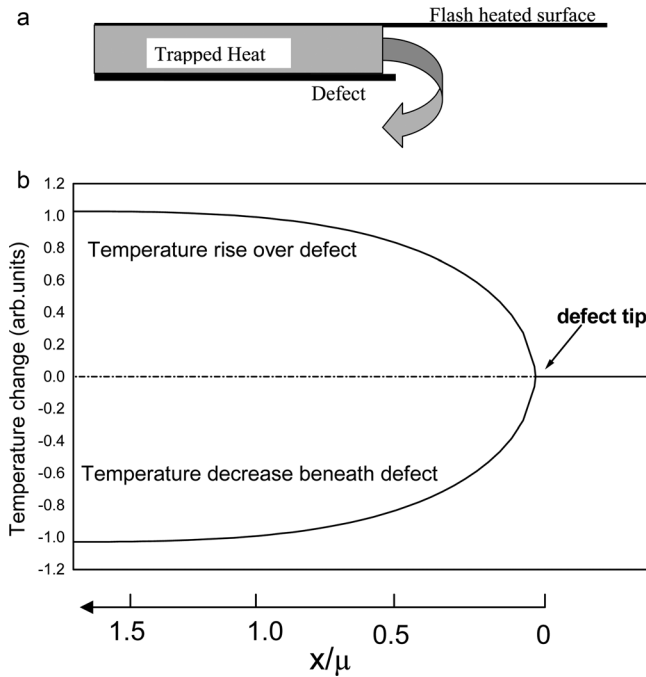


FIG. 1. (a) Schematic diagram of heat flow around the tip of a sub-surface in-plane defect following flash heating of the surface above the defect. (b) Temperature profiles along the upper and lower surfaces of a defect following flash heating of the surface above the defect. Temperature changes indicated are with respect to a sound region beyond the defect tip at the same depth and at the same time. The reduced distance from the crack tip is  $x/\mu$ , where  $\mu = 2\sqrt{\alpha t}$  the effective thermal diffusion length for a transient response.

function of the reduced distance,  $x/\mu$ , from the crack tip, where  $\mu$  is the effective thermal diffusion length, which is  $2\sqrt{\alpha t}$  for a transient response to a Dirac delta function excitation. Consequently, the actual range of the change in temperature at a crack tip expands with time elapsed after flash excitation. Figure 1(b) shows the thermal enhancement over a defect, caused by its blocking of thermal conduction, to be balanced by a reduction in heating below the defect, caused by the defect “shadowing” the heat being conducted from the surface. These phenomena result in high thermal gradients around the tip of the defect that drive the lateral thermal diffusion of the excess heat trapped between the surface and upper defect surface. This results in a cooling of the temperature enhancement at the surface over the defect, which is observed as a thermal contrast in flash thermography. This lateral conduction of heat to the defect tip is the dominant factor in determining the decay with time of a defect’s thermal contrast. It also affects the magnitude of the peak thermal contrast at the surface over a defect that has a particular size and aspect ratio.

Until now, it has been assumed that heat flow around a defect, following impulse surface heating, is a complex three-dimensional problem that can best be dealt with using numerical modelling techniques.<sup>10–12</sup> However, we will present here a simple analytical adaptation of Eq. (3) that appears to duplicate numerical modelling results for the magnitude of the peak contrast at the surface over a defect and its occurrence time. The key physical assumption is that the evolution of the thermal contrast over the centre of a defect is limited by the rate of lateral diffusion of heat from the centre to the defect edge. For a circular defect of diameter  $D$ , the diffusion distance is  $D/2$ . This lateral diffusion process competes with the build up of thermal contrast,  $T_{c1}(0, t)$ , caused by the through thickness thermal blocking of the defect

$$T_{c1}(0, t) = \frac{2J_0}{\sqrt{\pi\rho ckt}} \left[ \sum_{n=1}^{\infty} R^n e^{-\frac{(nd)^2}{\alpha t}} \right] \left( \right) \quad (5)$$

obtained from Eq. (3). This is the thermal contrast that will be observed for defects having very large lateral extent ( $D \gg d$ ), for which the lateral diffusion effects to the defect edges will be negligible. In the limit of an adiabatically isolated layer of thickness  $d$  absorbing an impulse of energy  $J_0$ , it is easy to see that its ultimate temperature rise, at long times will be  $J_0/\rho c d$ . Expression (5) rises asymptotically towards this value with time if  $R$  is set = 1 and a large number of the terms in the sum are computed. However, for lower aspect ratio defects, lateral thermal diffusion will reduce this thermal contrast significantly. The central hypothesis of this paper is that a better representation of the contrast at the surface over the centre of a circular defect, diameter  $D$ , at a depth  $d$  is

$$T_{c2}(0, t) = \frac{2J_0}{\sqrt{\pi\rho ckt}} \left[ \sum_{n=1}^{\infty} R^n e^{-\frac{(nd)^2}{\alpha t}} \right] \left( 1 - e^{-\frac{(D/2)^2}{4\alpha t}} \right) \left( \right) \quad (6)$$

In expression (6), the one-dimensional contrast term, Eq. (5), has been multiplied by a decay term to capture the physics of

the diffusion of heat from the centre of the circular defect to the edge, a distance  $D/2$  away. It assumes that the defect edge acts as a heat sink, sweeping away heat ( $\propto e^{-\frac{(D/2)^2}{4\alpha t}}$ ) reaching the edge around the high thermal gradients at the defect tip to the cool underside of the defect. Consequently, the heat remaining at the centre falls by the same amount. It is recognised that this is not a rigorous derivation, but it will be shown that the resulting expression, Eq. (6), provides a remarkably accurate approximation of the peak thermal contrast and its occurrence time after impulse heating.

Setting defect aspect ratio,  $P = D/d$ , Eq. (6) can be re-expressed as

$$Tc_2(0, t) = \frac{2J_0}{\sqrt{\pi\rho ckt}} \left[ \sum_{n=1}^{\infty} R^n e^{-\frac{(nd)^2}{4t}} \right] \cdot \left( 1 - e^{-\frac{(Pd)^2}{16\alpha t}} \right) \quad (7)$$

Layered carbon or glass fibre composites are important types of material that are inspected using flash thermography. For these, in-plane and through thickness thermal properties may differ substantially. Typically, in-plane thermal diffusivity is several times larger than through thickness thermal diffusivity. If the ratio of in-plane to through thickness thermal diffusivity is set  $= m$ , Eq. (7) becomes

$$Tc_2(0, t) = \frac{2J_0}{\sqrt{\pi\rho ckt}} \left[ \sum_{n=1}^{\infty} R^n e^{-\frac{(nd)^2}{4t}} \right] \cdot \left( 1 - e^{-\frac{(Pd)^2}{16m\alpha t}} \right) \quad (8)$$

It can be seen from Eq. (8) that an enhanced of in-plane/lateral diffusivity increases the diffusion rate of heat to the defect edge and, consequently, reduces the thermal contrast of a defect at a depth  $d$  of a particular aspect ratio  $P$ .

It is well known<sup>10,12,13</sup> that the contrast of small low aspect ratio defects peaks at a short time after flash heating. At such short times, the first  $n = 1$  term in the sum dominates the contrast given by Eq. (8). A useful indication of the way, in which the contrast of such small low aspect ratio defects changes with defect aspect ratio,  $P$ , and the anisotropy factor,  $m$ , can be obtained by taking the  $n=1$  term alone, and setting  $R = 1$ .

$$Tc_2^1(0, t) = \frac{2J_0}{\sqrt{\pi\rho ckt}} \left[ e^{-\frac{d^2}{4t}} \right] \cdot \left( 1 - e^{-\frac{(Pd)^2}{16m\alpha t}} \right) \quad (9)$$

From which, by setting  $y = \frac{d^2}{4t}$  and  $a = \frac{P^2}{16m}$ , it can be seen that

$$Tc_2^1(0, t) \propto e^{-y}(1 - e^{-ay}). \quad (10)$$

This expression peaks where

$$e^{-ay} = \frac{1}{(1+a)} \quad (11)$$

By inserting the resulting value of  $y$  in Eq. (10), it can be shown that peak contrast is a function of the term  $a$

$$Tc_{peak} \propto T(a) = \frac{a}{(1+a)^{\frac{1+a}{a}}}, \quad (12)$$

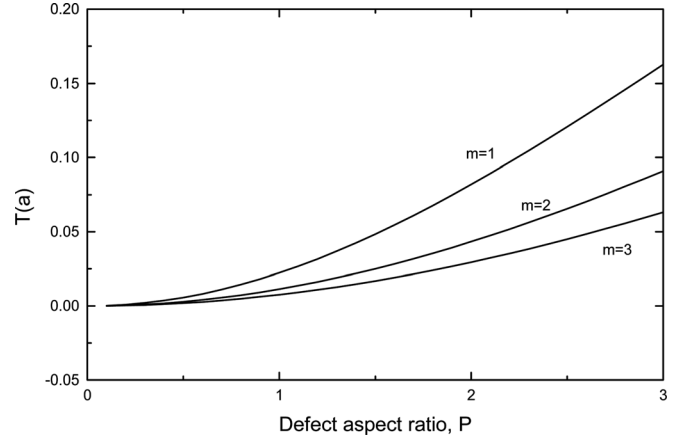


FIG. 2. Graph showing the variation of the peak thermal contrast function  $T(a)$ , from Eq. (12), with defect aspect ratio  $P$ , for the anisotropies,  $m$ , indicated.

where  $a < 1$

$$T(a) \approx \frac{a}{2} = \frac{P^2}{32m}, \quad (13)$$

i.e., peak contrast rises as the square of defect aspect ratio,  $P$ , and falls with thermal diffusivity anisotropy,  $m$ .

The dependence of  $T(a)$  on aspect ratio,  $P$ , for three values of thermal diffusivity anisotropy,  $m$ , is shown in Figure 2.

Whilst  $T(a)$  gives some insight into the low aspect ratio dependence of contrast, it is an incomplete description because it fails to include the  $t^{-0.5}$  term in Eq. (9).

Equation (9) can be re-expressed as a function of  $y$

$$Tc_2^1(0, y) = \frac{J_0}{d\rho c} \cdot \frac{2}{\sqrt{\pi}} \cdot \sqrt{y} \cdot [e^{-y}(1 - e^{-ay})] = \frac{J_0}{d\rho c} \cdot T(a, y). \quad (14)$$

In this expression,  $T(a, y)$  is the function that describes the extent of the deviation from the equilibrium isolated layer temperature rise,  $J_0/d\rho c$ , caused by lateral diffusion and thermal response time. It is an expression that peaks like  $T(a)$  at a values of  $y$  corresponding to the time at which there is a peak in thermal contrast, ( $y = d^2/4t$ ). These peak values of  $T(a, y)$  are functions of defect aspect ratio and thermal diffusivity anisotropy and they give an estimation of peak thermal contrast for the case of low aspect ratio defects. The dependences of the peak values of  $T(a, y)$  on aspect ratio,  $P$ , for three values of thermal diffusivity anisotropy,  $m$ , are shown in Figure 3. The forms of these graphs are very similar to those of Figure 2, showing that the  $t^{-0.5}$  term has a rather minor effect. The quadratic dependence on aspect ratio and the inverse dependence on diffusivity anisotropy, Eq. (13), are evident.

The time at which peak contrast appears,  $t_p$ , can be obtained from the values of  $y$ ,  $y_p$ , at which  $T(a, y)_{peak}$  occurs

$$t_p = \frac{d^2}{\alpha} \cdot y_p^{-1}. \quad (15)$$

The dependence of  $y_p^{-1}$  on aspect ratio,  $P$ , for three values of thermal diffusivity anisotropy,  $m$ , is shown in Figure 4. All



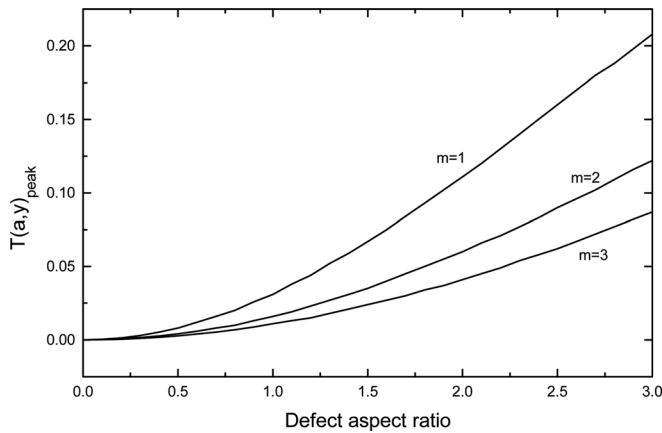


FIG. 3. Graph showing the variation of the peak thermal contrast function  $T(a,y)_{peak}$  from Eq. (14), with defect aspect ratio  $P$ , for the anisotropies,  $m$ , indicated.

three traces converge on a  $y_p^{-1}$  value of 0.67 at lowest defect aspect ratios.

Expressions (14) and (15) provide quantifications of the two most important parameters in pulsed thermographic non-destructive evaluation (NDE): the peak contrast that can be expected for a defect of specific size and depth and the time after the pulse excitation that this should occur. The first of these, peak contrast, provides an indication of the likelihood of detecting such a defect. Both expressions identify the ways, in which materials properties affect the performance of the inspection technique. The first, Eq. (14), shows thermal contrast to depend only on the density heat capacity product,  $\rho c$ , which varies rather little between material types. This accounts for the wide applicability that has been established for the technique. The thermal conductivity, which varies enormously between material types does not affect the magnitude of thermal contrast. Its effect is in the determination of the time that contrast peaks, through the inverse diffusivity relationship in expression (15). The dimensionless expressions  $T(a,y)_{peak}$  and  $y_p^{-1}$  incorporate the effects of defect aspect ratio and thermal diffusivity anisotropy. However, it is important to note that defect depth,  $d$ , appears separately outside these expressions, indicating that it is not only defect aspect ratio that limits thermal contrast. This

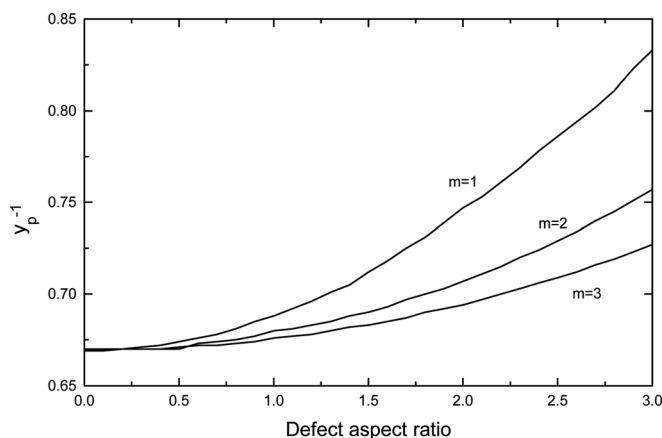


FIG. 4. Graph showing the variation of the peak contrast time function  $y_p^{-1}$  from Eq. (15), with defect aspect ratio  $P$ , for the anisotropies,  $m$ , indicated.

draws into question the supposed universal validity of the flash thermography rule-of-thumb that defect aspect ratio needs to exceed two.

The analytical results that have been introduced in this section are based on the proposal that the one-dimensional layer model, Eq. (3), should be modified as Eq. (8) to account for the three-dimensional heat flow effects that occur around a finite defect. The value of this analysis is tested in Sec. III by making a direct comparison between the analytical predictions and those obtained by detailed numerical modelling of the three-dimensional heat flow around the same defects.

### III. NUMERICAL MODELLING

The finite difference numerical modelling technique was used to compute the thermal response to impulse heating of a test piece containing circular plate-like air filled defects set in a plane parallel to the surface. The finite difference modelling code was written using cylindrical co-ordinates to enable the 3-D heat conduction process to be solved using a 2-D numerical model.<sup>10</sup> The implicit backward Euler method was used. 7000 time steps were used across the time range considered (a cooling transient of 3 s for steel and 10 s for carbon fibre composite). The Dirac excitation pulse was simulated by a triangular impulse, three time steps in duration, to prevent oscillatory behaviour due to step heating derivatives. A spatial grid of 100 radial steps and 300 through thickness steps was employed.

Results were obtained for mild steel and a carbon fibre composite material, representing relevant isotropic and anisotropic materials that might be inspected using flash thermography.

#### A. Mild steel

The thermal properties of mild steel used in the numerical modelling are shown in Table I.

Modelling results were obtained for defects with diameters between 0.25 and 30 mm all at a depth of 1 mm below the surface, covering defect aspect ratios from 0.25 to 30. The surface was subjected to a uniform intensity of  $10^6 \text{ W m}^{-2}$  for 10 ms, approximating an impulse heating of  $10 \text{ kJ m}^{-2}$  that is comparable to impulse heating amplitudes employed in flash thermography.<sup>13–15</sup> The thermal contrast at the centre of the simulated defect images was obtained at 10 ms intervals for a period of 0.5 s after applying the impulse heating.

The peak values for thermal contrast obtained by the numerical modelling are shown in Figure 5. Values for diameters between 0.25 and 1 mm were obtained at intervals of 0.05 mm. These values were used to generate the lower part of the graph and are shown without symbols for clarity. The predictions of the analytical expression, Eq. (8), across the defect aspect ratio range 0.3 to 30 are also shown in the figure

TABLE I. Thermophysical properties of mild steel.

Density ( $\text{kg/m}^3$ )	Specific heat ( $\text{J kg}^{-1} \text{K}^{-1}$ )	Thermal conductivity ( $\text{W m}^{-1} \text{K}^{-1}$ )
7832	434	64

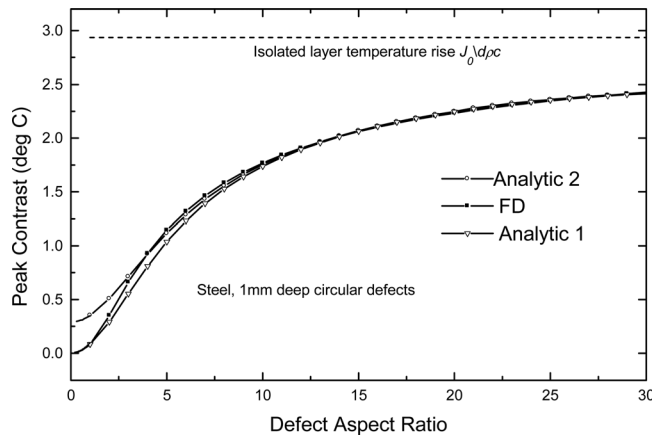


FIG. 5. Variation of peak thermal contrast with defect aspect ratio for circular defects 1 mm beneath the surface of a mild steel sample. Pulse intensity  $10 \text{ kJ m}^{-2}$ .

(Analytic 1) for comparison. The range 0.3 to 1.0 was covered in steps of 0.1 and again these points are plotted without symbols for clarity and to allow comparison with the numerical modelling in this range, detailed as mentioned above. The values of Eq. (8) were obtained by including the first six ( $n = 1$  to 6) terms of the sum in Eq. (8) and the thermal reflection coefficient  $R$  was set to 1. It was found that no significant increase in contrast was obtained on including more than the first six terms of the sum for defect aspect ratios up to 30. Equation (8) reproduces the overall form of the dependence of contrast on defect aspect ratio obtained by numerical modelling. It provides a very good approximation of numerical modelling results for defect aspect ratios below 2 and above  $\sim 8$ . Between these values, it underestimates contrast, indicating that the decay expression Eq. (8) should be somewhat weaker for intermediate values of defect aspect ratio.

The second analytical curve (Analytic 2) shown in Figure 5 was obtained by a minor modification of Eq. (8). This was to raise the diffusion distance from the point on the surface above the centre of the defect edge from  $D/2$  to the true distance  $\sqrt{[(D/2)^2 + d^2]}$ . The result is a better fit to the numerical modelling results for all defect aspect ratios above  $\sim 3$ , but a serious overestimation for low defect aspect ratios. This indicates a subtle difference in thermal diffusion processes for small defects.

The adiabatically isolated layer equilibrium temperature rise  $J_0/\rho c d$  is shown at the top of Figure 5. This value is approached asymptotically as defect aspect ratio is increased in both the analytical and finite difference modelling and it provides a means of validating these models. The functional form of the peak contrast vs. defect aspect ratio graph is the equivalent of  $T(a,y)_{\text{peak}}$  introduced above; representing the reduction in contrast from  $J_0/\rho c d$  caused by lateral diffusion of heat to the crack edges.

Peak contrast times obtained using the analytical model (Analytic 2) are compared with the values indicated by the finite difference modelling in Figure 6. The agreement is within 5%, across the 3 to 30 defect aspect ratio range, showing the analytical model to provide a useful indication of both peak contrast and peak contrast time for a wide range of defect geometries.

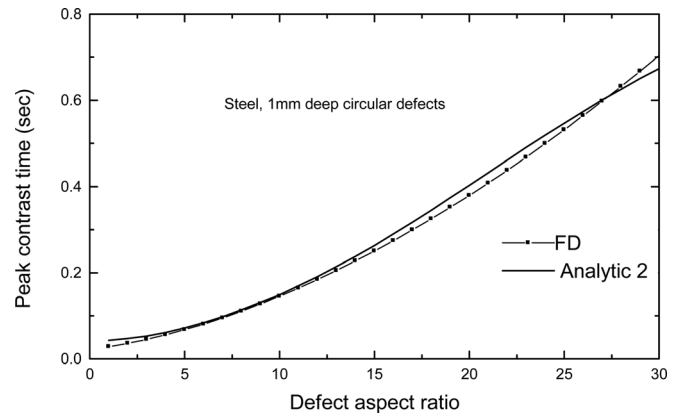


FIG. 6. Variation of peak contrast time with defect aspect ratio for circular defects 1 mm beneath the surface of a mild steel sample.

The developments of thermal contrast with time can also be obtained from the analytical model, Eq. (8). Examples, defect aspect ratios of 5, 10, and 15, are shown in Figures 7(a)–7(c). The results in Figure 7 show that the modified form of Eq. (8) (Analytic 2) accurately predicts the time dependence of contrast up to the peak. However, at longer times, the analytical expression for contrast decays less rapidly than indicated by numerical modelling. This is probably a result of the high thermal gradients driving lateral thermal diffusion receding towards the defect centre as the trapped heat is conducted away from the defect edges with time.

## B. Carbon fibre composite material

The thermal properties of a representative carbon fibre composite material used in the numerical modelling are shown in Table II.

Modelling results were obtained for defects with diameters between 1 and 30 mm all at a depth of 1 mm below the surface, covering defect aspect ratios from 1 to 30. The surface was again subjected to a uniform intensity of  $10^6 \text{ W m}^{-2}$  for 10 ms, approximating an impulse heating of  $10 \text{ kJ m}^{-2}$  that is comparable to impulse heating amplitudes employed in flash thermography. The thermal contrast at the centre of the simulated defect images was obtained at 10 ms intervals for a period of 10 s after applying the impulse heating.

The peak values for thermal contrast obtained by the numerical modelling and the two forms of the analytical model are shown in Figure 8. The characteristics of the three curves are similar to those for steel shown in Figure 5. However, the rate of increase in peak contrast with defect aspect ratio is noticeably lower due to the anisotropy in thermal diffusivity of 3 that enhances the cooling of thermal contrast above a defect. The relative magnitudes of peak contrast for specific aspect ratio defects, compared with the isolated layer temperature rise, are lower than seen for steel for the same reason. There is a significant discrepancy between the predictions of the first analytical model, Eq. (8), (Analytic 1) and the finite difference modelling for aspect ratios between 3 and 12. The modified analytical model agrees well with the numerical modelling results for aspect ratios above 5. The discrepancies between the analytical and numerical modelling results are somewhat larger than found, Figure 5, for steel. It is notable

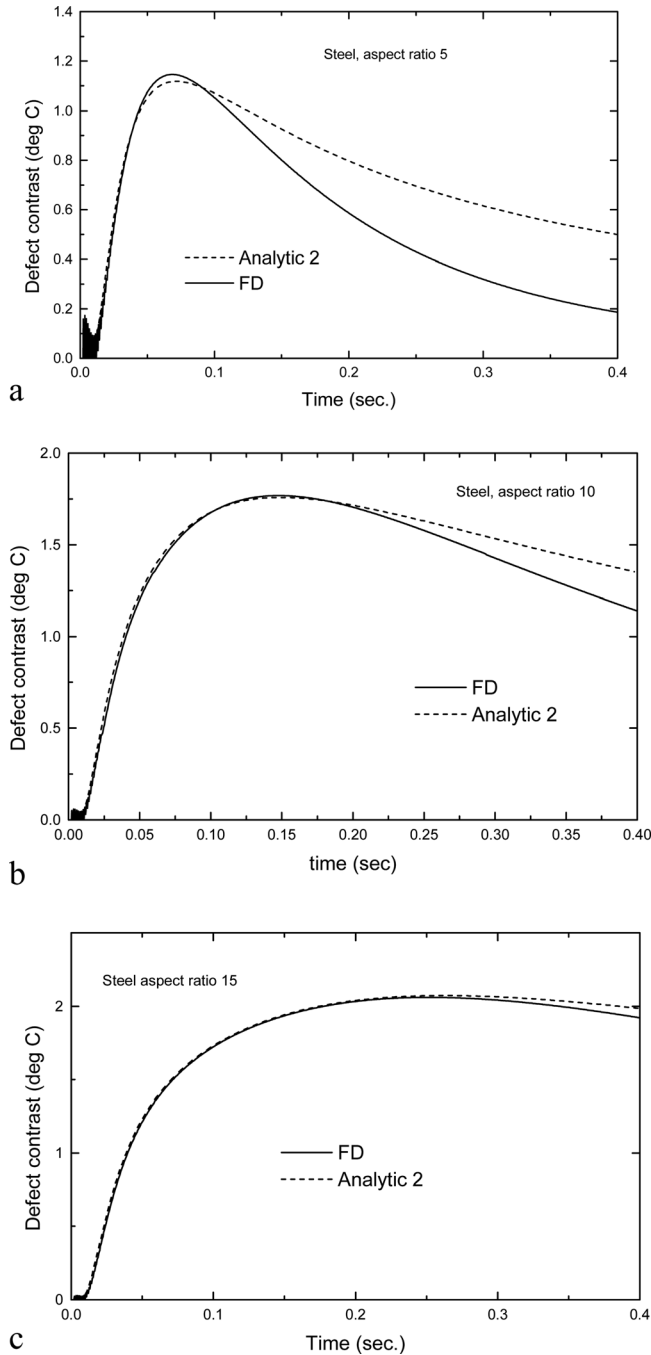


FIG. 7. Thermal contrast vs. elapsed time for a (a) 5, (b) 10, and (c) 15 mm diameter defects 1 mm beneath the surface of a mild steel sample calculated by finite difference modelling (FD) and the modified form of Eq. (8) (Analytic 2). Pulse intensity  $10 \text{ kJ m}^{-2}$ .

that there is rather little difference in the predicted magnitudes of peak contrast for steel and carbon fibre composite, despite the huge difference in their thermal conductivities (a factor of 100). This is in agreement with the assertion (Sec. II) that

TABLE II. Thermophysical properties of a carbon fibre composite material.

Density ( $\text{kg/m}^3$ )	Specific heat ( $\text{J kg}^{-1} \text{K}^{-1}$ )	Thermal conductivity ( $\text{W m}^{-1} \text{K}^{-1}$ )	Diffusivity anisotropy, m
1500	1200	0.64	3

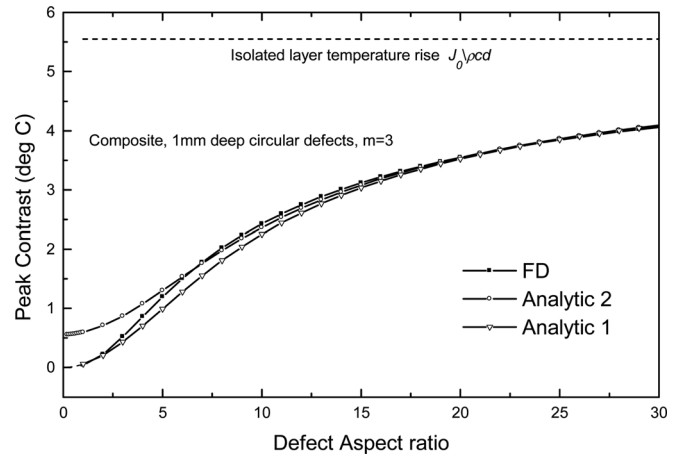


FIG. 8. Variation of peak thermal contrast with defect aspect ratio for circular defects 1 mm beneath the surface of a carbon fibre composite sample. Pulse intensity  $10 \text{ kJ m}^{-2}$ .

thermal contrast magnitude depends only on the  $\rho c$  product and it is independent of thermal conductivity.

Peak contrast times obtained using both analytical models (Analytic 1 & 2) are compared with the values indicated by the finite difference modelling in Figure 9. The agreement is fairly good across the 0 to 30 defect aspect ratio range, though not as good as found for isotropic steel. The times of the contrast peaks in the composite are very much longer than predicted for steel, supporting the inverse diffusivity indication of Eq. (15).

The developments of thermal contrast with time for defect aspect ratios of 5, 10, and 15 in a carbon fibre composite are shown in Figures 10(a)–10(c). The results in Figure 10 again show that the modified form of Eq. (8) (Analytic 2) reproduces the early part of the time dependence of thermal contrast indicated by the numerical modelling. As for steel at longer times, the analytical expression decays less rapidly than indicated by numerical modelling.

#### IV. EXPERIMENTAL RESULTS

A Thermal Wave Imaging Inc. thermoscope system<sup>16</sup> was used to measure the contrast produced by artificial defects in the form of circular flat bottomed holes drilled to a

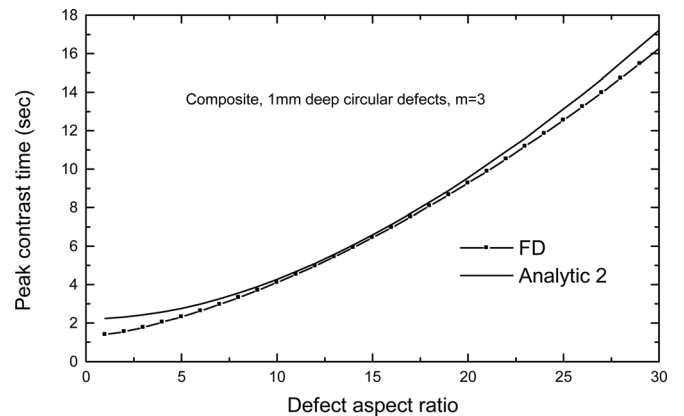


FIG. 9. Variation of peak contrast time with defect aspect ratio for circular defects 1 mm beneath the surface of a composite sample.



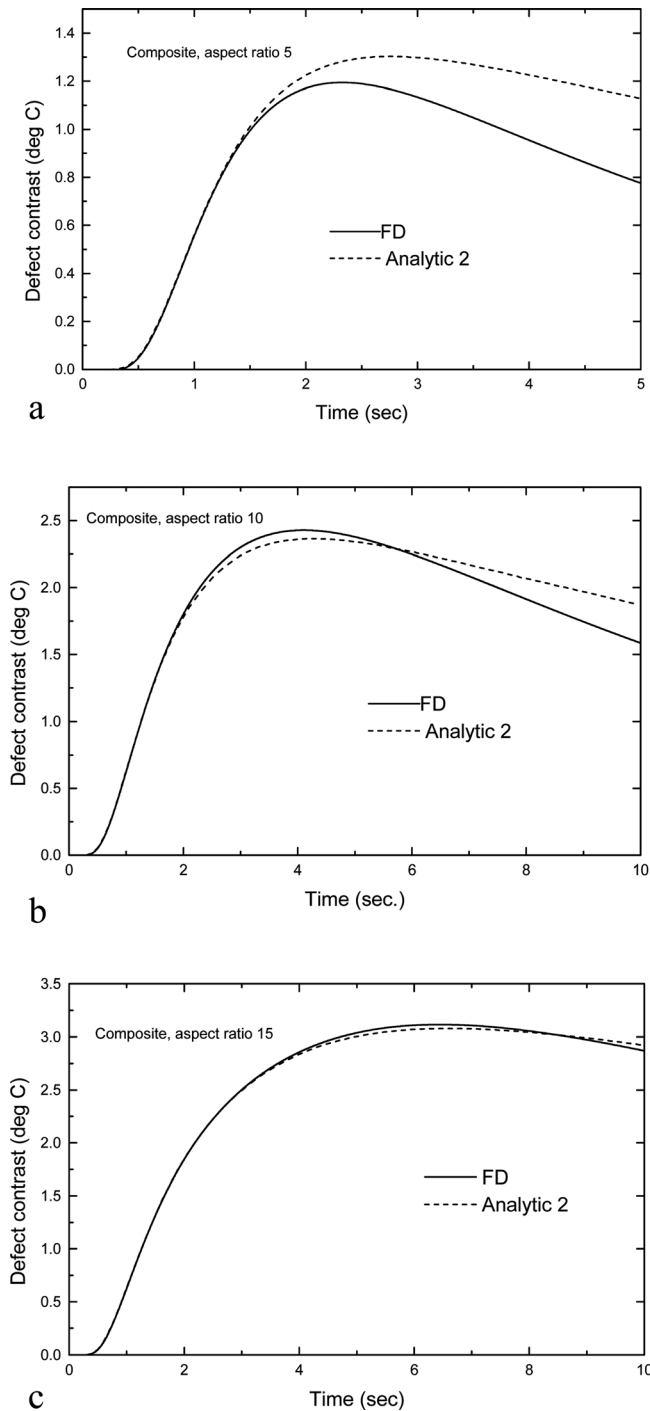


FIG. 10. Thermal contrast vs. elapsed time for a (a) 5, (b) 10, and (c) 15 mm diameter defects 1 mm beneath the surface of a carbon fibre composite sample calculated by finite difference modelling (FD) and the modified form of Eq. (8) (Analytic 2). Pulse intensity  $10 \text{ kJ m}^{-2}$ .

depth of 1 mm from the surface of a mild steel plate. The upper surface of the plate was painted black. It is appreciated that flat bottomed holes differ from the true lamina defects illustrated in Figure 1 and that for these, there is no path for the heat to flow to the cooler underside of the defect. However, numerical modelling comparisons of the two types of sub-surface feature indicate the flat bottomed hole to act as a good approximation to the real lamina crack-like defect, in this case. For an aspect ratio 5 defect in steel at a depth of 1 mm, the contrast over a flat bottomed hole is 6.3% larger

than over a lamina crack-like defect and for the aspect ratio of 10, the difference falls to 2.3%. Each of the artificial defects was positioned in the same place beneath the flash hood to ensure that they received the same excitation intensity. The experimental measurements of the peak value of contrast obtained from each of the artificial defects are shown in Figure 11(a). The holes had diameters in the range 1 to 18 mm to cover the defect aspect ratio range 1 to 18.

The analytical curve through the experimental data was obtained from Eq. (8), setting the absorbed thermal flux,  $J_0$ , to  $3.3 \text{ kJ m}^{-2}$ . Note, no image of the 1 mm diameter hole was obtained. The times of occurrence of peak contrast are shown in Figure 11(b). The analytical curve through the data was obtained from the analytical model using a value of  $45 \text{ W m}^{-1} \text{ K}^{-1}$  for the thermal conductivity of the mild steel plate. This is lower than the nominal value shown in Table I, but within the range of values expected for carbon steels.

## V. DISCUSSION

The comparison of analytical and numerical modelling results presented in Sec. III shows that the simple analytical expression, Eq. (8), introduced in Sec. II provides good estimates of the magnitude of the thermal contrast, and its

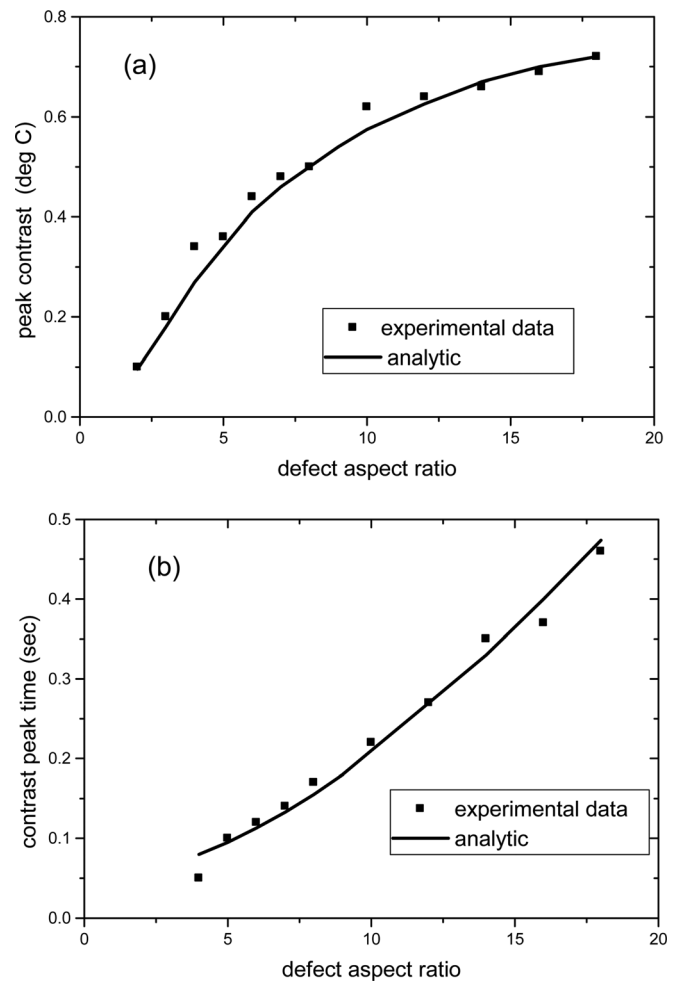


FIG. 11. Experimental measurements of: (a) peak contrast in a mild steel plate of circular flat bottomed holes of diameters in the range 2 to 18 mm all at a depth of 1 mm from the surface and (b) times of peak contrast compared with the predictions of the analytical expression.

occurrence time, for a wide range of defect aspect ratios. The variation in thermal contrast with defect aspect ratio is smooth and systematic and it can be related in a simple and clear way to materials properties. The analytical model has been shown to provide a rapid and simple means of assessing the likely performance of the flash thermography NDE technique. It reproduces the salient features of more detailed numerical modelling, which requires considerable expertise to ensure reliability of results. The analytical model has also revealed systematic dependencies of contrast and peak contrast time on defect geometry and materials properties that had not been noticed in previous numerical modelling studies.

In this work, it has been assumed that the defects have very high thermal contact resistances preventing heat from being conducted through the defects to the underlying bulk. In the analytical model, the effective thermal reflection coefficient at the defect surface  $R$  was set equal to 1. In this case, the results show the effects on contrast of the lateral diffusion of heat to the defect edge alone. The contrast predictions are consequently an upper limit of what might be observed in practice where some defects may have very small openings and associated small thermal contact resistances. In such cases, there will be little trapping of heat at the surface above the defect and a much reduced thermal contrast at the surface.

An important question that must be answered to determine the suitability of flash thermography for a specific inspection application is whether the technique will reveal the presence a defect of a required minimum size within a component of a particular thickness made of a specified material. For such a defect to be detected, it is necessary for the peak contrast, it produces to exceed the noise level of the IR camera to be employed in the inspection. The intrinsic noise levels of the IR cameras typically employed in flash thermographic NDE are quoted as  $\sim 0.02^\circ\text{C}$ . However, practical experience indicates that contrasts of  $\sim 0.1^\circ\text{C}$  are necessary to produce reliable distinguishable images of sub-surface defects. Equation (8) provides a simple means of making this assessment, provided the pulse excitation energy,  $J_0$ , is known. The value of  $10\text{ kJ m}^{-2}$  employed in the simulations here is representative of the magnitude of  $J_0$  achieved by the type of flash lamps used for flash thermography. The actual value of  $J_0$  in a particular application can be obtained by fitting Eq. (2) to the thermal decay observed in a defect free region of the test piece of interest.

Examination of the contrasts predicted for steel and composite shown in Figures 5 and 8 appears to confirm the flash thermography rule-of-thumb as peak contrasts fall below above mentioned minimum required contrast of  $0.1^\circ\text{C}$  where the defect aspect ratio falls below about 2. However, this is coincidental and a consequence of performing the simulations for defects set at a depth of 1 mm. The amplitude of contrast is expected to scale as a fraction of the equilibrium isolated layer temperature rise  $J_0/d\rho c$ , i.e., inversely with defect depth  $d$ . If the defect depth was 10 mm, the magnitudes of the contrasts shown in Figures 5 and 8 would be reduced by a factor of 10. For this depth, only defects with aspect ratios above  $\sim 5$  would exhibit contrast exceeding the reliability threshold of  $0.1^\circ\text{C}$ . Defects of aspect ratio 2 would show a contrast of only  $\sim 0.03^\circ\text{C}$ . This inverse depth relationship has been

confirmed by finite difference modelling. Similarly, the  $d^2$  increase in peak contrast time, Eq. (15), has also been confirmed by independent numerical modelling.

The effect of the inverse depth relationship and the consequent general incorrectness of the rule-of-thumb have been exposed by attempts at imaging the artificial defects in the test piece shown in Figure 12. Whilst the rule-of-thumb would suggest that all these defects would be imaged, only the shallowest, 2 mm deep, was imaged very weakly. The predictions of the peak contrasts for the test piece that take account of the defect depth and actual absorbed pulse energy are shown at the foot of the figure. Only the shallowest, 2 mm deep, defect is predicted to produce a contrast significantly above camera noise level ( $\sim 0.02^\circ\text{C}$ ), explaining the absence of images of the other deeper defects. The 2 mm diameter, 1 mm deep, defect was found to exhibit a peak contrast of  $\sim 0.1^\circ\text{C}$  in the study of 1 mm deep defects in mild steel, results shown in Fig. 11(a).

The value of the analytical expression, Eq. (8), is that it provides the key information about the flash thermography technique in a simple and accessible form. The alternative of using numerical modelling is time consuming and its reliability and validity is highly dependent on the experience and expertise of the modeller. The analytical model provides the basis for an expert system that could be developed to be used by non-specialists to assess the suitability of flash thermography for a particular inspection application. System inputs would be defect depth, minimum required detectable defect size, and material properties. The principal output would be peak defect image contrast that could be compared directly with a system noise threshold, such as  $0.1^\circ\text{C}$ , to ascertain the suitability of the technique for the required inspection.

Whilst the analysis presented here has focussed on the flash thermography NDE technique, the impulse response that has been obtained can be used to model other modes of excitation. It is a simple matter to integrate a series of impulse responses to simulate long pulse heating. A useful alternative to flash lamp heating is to expose a test piece surface to a high power lamp or a hot air blower for a number of seconds and then monitor the cooling with an IR camera. Similarly, the response to a periodically modulated heat

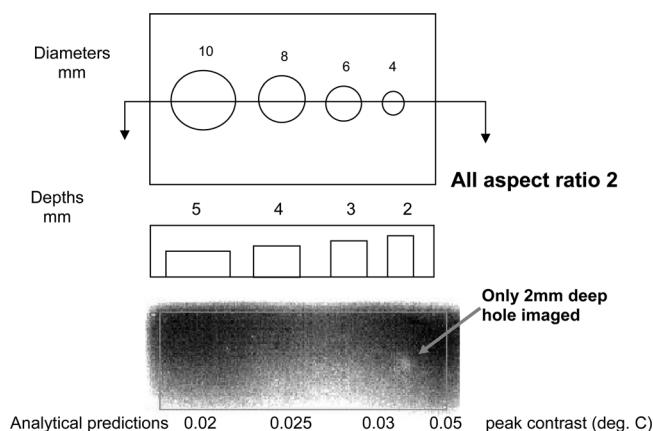


FIG. 12. Drawing of mild steel test piece with aspect ratio 2 defects at depths 2 to 5 mm from the surface. Thermal image below shows a weak image of only the 2 mm deep hole.

source, of the type used in lock-in thermography, can be modelled by the integration of a series of periodically modulated amplitude impulse responses. It is becoming common to process flash thermography image files to generate first or second time derivative images<sup>17–19</sup> as these images have been shown to be clearer than the raw flash thermography images and to reveal defects that do not appear in the raw images. These time derivative imaging methods make particular use of the early part, pre-contrast-peak part, of the thermal response. Figures 7 and 10 show that this is where the analytical model produces the most accurate agreement with the full numerical modelling predicted response. Consequently, the model can be used with some confidence to investigate the characteristics of the time derivative imaging methods. There have been no systematic investigations, of the type presented here for flash thermography, of these other thermographic NDE methods but these will be dealt with in future publications.

## VI. CONCLUSIONS

A simple analytical expression has been discovered that has been shown to model the dependence of flash thermography image contrast on defect aspect ratio. This expression shows that the defect detection sensitivity of the technique does not depend on aspect ratio alone. It increases with the absorbed excitation pulse energy  $J_0$  and it is inversely proportional to defect depth  $d$ . Consequently, it is concluded that the long established thermographic NDE rule-of-thumb that links defect detection sensitivity to aspect ratio alone is incorrect. Furthermore, it has been shown experimentally that the rule-of-thumb is misleading, providing compelling

evidence for its abandonment in light of the far more complete analytical treatment of defect detection sensitivity presented here.

## ACKNOWLEDGMENTS

This work formed part of the Core Research Programme of the UK Research Centre in NDE supported by the Engineering and Physical Research Council, UK. One of the authors (DPA) wishes to acknowledge the stimulating discussions with Dr. S. M. Shepard that lead to this work.

<sup>1</sup>J. M. Milne and W. N. Reynolds, Proc. SPIE **520**, 119 (1984).

<sup>2</sup>W. N. Reynolds and G. M. Wells, Br. J. Non-Destr. Test. **40**, 256 (1984).

<sup>3</sup>J. M. Milne and W. N. Reynolds, Proc. SPIE **590**, 293 (1985).

<sup>4</sup>H. S. Carslaw and J. C. Jaeger, *Conduction of Heat in Solids*, 2nd ed. (Oxford University Press, 1959).

<sup>5</sup>S. K. Lau and D. P. Almond, J. Phys. D: Appl. Phys. **24**, 428 (1991).

<sup>6</sup>D. P. Almond and P. M. Patel, *Photothermal Science and techniques* (Chapman-Hall, 1996).

<sup>7</sup>C. A. Bennett and R. R. Patty, Appl. Opt. **21**, 49 (1982).

<sup>8</sup>D. P. Almond and S. K. Lau, Appl. Phys. Lett. **62**, 3369 (1993).

<sup>9</sup>D. P. Almond and S. K. Lau, J. Phys. D: Appl. Phys. **27**, 1063 (1994).

<sup>10</sup>M. B. Saintey and D. P. Almond, J. Phys. D: Appl. Phys. **28**, 2539 (1995).

<sup>11</sup>M. Krishnapillai, R. Jones, H. Marshall, M. Bannister, and N. Rajic, Compos. Struct. **75**, 241 (2006).

<sup>12</sup>V. P. Vavilov, Proc. SPIE **3700**, 14 (1999).

<sup>13</sup>S. K. Lau, D. P. Almond, and J. M. Milne, NDT & E Int. **24**, 195 (1991).

<sup>14</sup>S. G. Pickering and D. P. Almond, NDT & E Int. **41**, 501 (2008).

<sup>15</sup>S. M. Shepard, J. R. Lhota, and T. Ahmed, NDT & E Int. **22**, 113 (2007).

<sup>16</sup>Thermal Wave Imaging, Inc. Ferndale, MI 48220 USA.

<sup>17</sup>S. M. Shepard, J. R. Lhota, B. A. Rubadeux, D. Wang, and T. Ahmed, Opt. Eng. **42**, 1337 (2003).

<sup>18</sup>S. M. Shepard, Proc. SPIE **5074**, 882 (2003).

<sup>19</sup>S. M. Shepard, Y. L. Hou, J. R. Lhota, and J. M. Golden, Opt. Eng. **46**, 510081 (2007).